Laser and Particle Beams (2014), *32*, 631–637.

doi:10.1017/S0263034614000652

Developments toward hard X-ray radiography on heavy-ion heated dense plasmas

K. LI,[1,2,6] B. BORM,[3] F. HUG,[4] D. KHAGHANI,[1,2] B. LÖHER,[1,2] D. SAVRAN,[1,2] N. A. TAHIR,[5] AND P. NEUMAYER[1,2]

[1]ExtreMe Matter Institute, GSI, Darmstadt, Germany
[2]Frankfurt Institute for Advanced Studies, Frankfurt am Main, Germany
[3]Goethe-Universität, Frankfurt am Main, Germany
[4]Institut für Kernphysik,TU Darmstadt, Darmstadt, Germany
[5]GSI Helmholtzzentrum für Schwerionenforschung GmbH, Darmstadt, Germany
[6]Joint Laboratory on High Power Laser and Physics, SIOM, Shanghai, China

(RECEIVED 14 August 2014; ACCEPTED 16 September 2014)

Abstract

We have studied the potential of hard X-ray radiography as a diagnostic in high energy density experiments, proposed for the future Facility for Antiproton and Ion Research (FAIR). We present synthetic radiographic images generated from hydrodynamic simulations of the target evolution. The results suggest that high-resolution density measurements can be obtained from powerful hard X-ray sources driven by a PW-class high-energy laser system. Test measurements of a prototype hard X-ray imaging detector for photon energies above 100 keV are presented.

Keywords: Hard X-ray radiography; Heavy-ion heating; High energy density; Warm-dense plasmas

INTRODUCTION

The upcoming facility for antiproton and ion research (FAIR), currently under construction at the Helmholtz Center for Heavy-Ion Research GSI (Darmstadt, Germany), will offer heavy ion beams at unprecedented intensities (Henning, 2004; Spiller & Franchetti, 2006). One of the research pillars within the multi-facetted scientific program at FAIR is the area of dense plasmas (Hoffmann *et al*., 2005). A variety of schemes has been proposed to generate matter at high energy density (HED) conditions using the intense ion pulses delivered by the FAIR accelerator complex (e.g., Tahir *et al*., 2005; 2010, Tauschwitz *et al*., 2009). This promises novel and unique approaches for accurate studies of matter under such extreme conditions, complementary to the highly non-equilibrium states produced with X-ray free electron lasers (e.g., Zastrau *et al*., 2012).

As a feature common to most of these schemes, the targets undergo a large hydrodynamic evolution, mostly in the so-called warm-dense matter (WDM) regime. In this regime, the equation-of-state is rather poorly known and theoretical modelling is a great challenge (e.g., Lomonosov, 2007) due to strong-coupling of the ions and partial electron degeneracy (which is, of course, also the main motivation for the experimental study of matter at WDM conditions). For this reason, accurate monitoring of the target density distribution is crucial to verify the target performance. Besides, density is an important plasma parameter, and, for example, conductivity measurements in the WDM regime are meaningless without accurate knowledge of the target density. Finally, in most equation-of-state experiments, the target hydrodynamic evolution, such as shock propagation or isentropic release is the primary observable. Thus, radiography to measure the target density distribution will be an indispensable key enabling diagnostic technique for HED experiments at the future FAIR facility.

In this paper, we explore the potential of radiography based on hard X-rays produced by intense high-energy laser pulses on solid targets for targets proposed for FAIR. This study is in context of current planning for a high-energy high-intensity laser system to be installed near the FAIR plasma physics experimental area, with the purpose to enable advanced diagnostic techniques. Furthermore, we present first test results from recent developments of hard X-ray imaging detectors particularly designed for use in such scenarios.

Address correspondence and reprint requests to: P. Neumayer, ExtreMe Matter Institute, GSI, Planckstr. 1, 64291 Darmstadt, Germany. E-mail: p.neumayer@gsi.de

RADIOGRAPHY OF DENSE PLASMAS USING PW-LASER GENERATED HARD X-RAY BREMSSTRAHLUNG

X-ray radiography using high-energy laser-produced plasmas as sources for intense X-ray radiation of some 10s of keV photon energy (see, e.g., Hicks *et al*., 2010; Kritcher *et al*., 2014) has become a routine tool in many HED laboratories. However, most of the target schemes proposed to produce HED samples at FAIR involve large (mm-size), dense high-Z targets. Photon energies suitable to penetrate such targets are in the 100 keV to MeV spectral range. Intense bursts of such energetic X-rays are emitted from solid targets irradiated by laser-pulses at relativistic intensities ($> 10^{18}$ W/cm^2). In the interaction of laser light at relativistic intensities with overdense plasma, a large fraction of laser energy is converted to hot (supra-thermal) electrons with energies reaching several times the ponderomotive energy $E_p = 511\ \text{keV} \times (1 + 0.73 \times I_{18}\lambda_\mu^2)^{1/2}$, where $I_{18} \times 10^{18}\ \text{W/cm}^2$ and $\lambda_\mu \times 1\ \mu\text{m}$ are the laser intensity and wavelength, respectively. Traversing the solid density target these fast electrons give rise to intense characteristic line emission (Park *et al*., 2006) and bremsstrahlung. The emission duration is limited by the relaxation of the hot electron population to picoseconds corresponding to the energetic electron stopping range (≈ mm) in matter at solid density (Nilson *et al*., 2012). This time is short compared to the hydrodynamic timescale, thus the hard X-ray emission is spatially restricted to the initial target dimensions. Using limited-size targets source sizes down to 10 μm have been demonstrated, allowing simple point-projection radiography schemes (Park *et al*., 2008). Point-projection radiography has the important advantage, that no imaging optics (lens, pinhole) is required, making it applicable up to very high photon energies, where no lenses are available and pinholes become transparent. This radiography scheme has successfully been employed, for example, to image laser-driven shocks (Brambrink *et al*., 2009; LePape *et al*., 2010), the isentropic expansion of isochorically heated wire-targets (Hochhaus *et al*., 2013) and direct-drive implosions of CH shells at the Omega Laser facility (Tommasini *et al*., 2011) and is being under consideration for implementation at the National Ignition Facility to measure the areal density of the highly-compressed fuel in inertial confinement fusion experiments. While most experiments were performed on low-Z targets of small areal density, measurements of the hard X-ray yield indicate that a large amount of high-energy (> 100 keV) bremsstrahlung is produced, suitable to penetrate large high-Z targets.

SIMULATIONS OF HARD X-RAY RADIOGRAPHY ON HED TARGETS FOR FAIR

In order to assess the potential of intense-laser driven hard X-ray radiography as diagnostic for HED experiments proposed for FAIR, we have simulated radiographic images. Here we have used results from hydrodynamic calculations presented by Tahir *et al*. (2005). In the proposed experiments, a solid lead cylinder (diameter 0.6 mm, length 2 mm) is placed in the focus of the heavy ion beam, with the cylinder axis aligned parallel to the ion beam. Transverse homogenous heating is ensured as the ion focal spot diameter is significantly larger than the target. As the stopping range of the relativistic heavy ions largely exceeds the target length energy deposition along the ion beam direction is very homogenous, resulting in a quasi-cylindrical geometry. Using the ion beam parameters anticipated at FAIR Tahir *et al*. (2005) could show that a wide range of high-entropy states can be accessed, ranging from hot liquid, over the two-phase liquid-gas regime and the region around the critical point, up to the regime of strongly coupled plasmas.

Figure 1a shows a schematic of a possible setup to perform X-ray radiographic measurements on this target. A thin (10 μm) "backlighter" foil is located at a distance of about 1 cm from the target and irradiated by the high-energy high-intensity laser pulse. Employing the radiation emitted from the edge of the foil results in a strongly astigmatic backlighting source. As explained above, emission in the direction normal to the foil is limited to the initial foil thickness (i.e., 10 μm). In the direction along the foil, the emission source

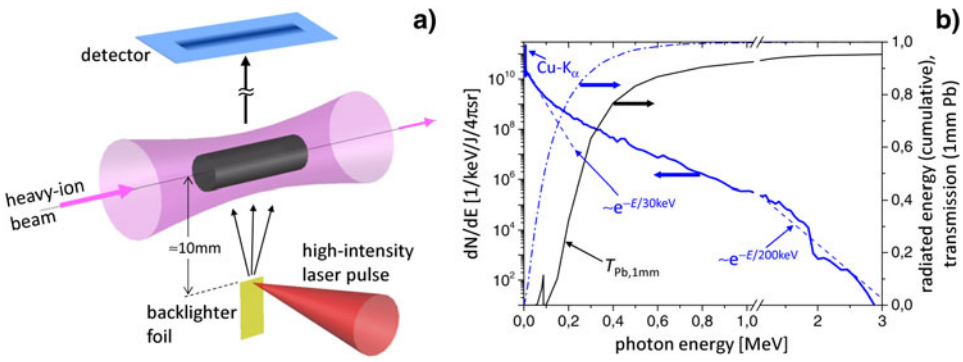

Fig. 1. (**a**) Schematic setup to perform laser-driven X-ray radiography on a heavy-ion heated sample. (**b**) Calculated bremsstrahlung emission spectrum (blue, solid) generated in the backlighter foil by the laser-generated supra-thermal electrons, and cumulated radiated energy (blue, dot-dashed). For comparison, the transmission through 1 mm of lead is plotted (black).

https://doi.org/10.1017/S0263034614000652 Published online by Cambridge University Press

size is rather determined by the transverse spreading of the hot electrons, which is typically of the order 100 μm, as inferred from X-ray imaging crystal spectrometers (e.g., Zastrau *et al*., 2010) or knife-edge tests (Hochhaus *et al*., 2013). By orienting the backlighter foil edge parallel to the cylinder axis, the transverse and longitudinal source sizes are well-matched to the characteristic length scales of the heavy-ion heated sample. The distance between source (foil edge) and target was chosen to limit the effective increase in transverse source size due to an oblique view onto the backlighter foil toward the edge of the required field-of-view. This distance, at the same time, determines the solid angle subtended by a resolution element in the target, and thereby the number of photons available in the corresponding pixel for image generation. X-ray emission spectra are calculated by a Monte-Carlo electron-photon transport code, using a 1-temperature hot electron spectrum with mean electron energy of 200 keV. In the widely used scaling by Beg *et al*. (1997), this corresponds to a focused intensity of about 10^{18} W/cm^2, and we have found reasonable agreement with our measurements of the hard X-ray yield (Neumayer *et al*., 2010).

Figure 1b shows the calculated emission spectrum, the number of photons per keV energy interval and per Joule of energy in the hot electron distribution, emitted into the full solid angle. At about 8 keV the copper K-alpha fluorescence can be observed as the target material used in the simulations was copper. The bremsstrahlung continuum emission initially falls off rather rapidly as $dN/dE \propto e^{-E/30\ \mathrm{keV}}$ up to about 100 keV. The slope gradually decreases until for photon energies beyond 1 MeV the slope approaches that of a 1-temperature distribution with a temperature of 200 keV. For comparison, we plot the transmission of a 1 mm thick lead target showing that photon energies well above 100 keV are required to penetrate the target. Also shown is the cumulative energy (normalized to 1) of the X-ray emission. We find close to 30% of the total emitted energy at photon energies between 100 keV and 200 keV, and another 10% into photons at 200–300 keV. The total radiated energy is about 0.8% of the hot electron energy. This value is in good agreement with the conversion efficiencies reported by Tommasini *et al*. (2011). Here we assume laser pulse energy of 400 J (which is the projected pulse energy for the laser system under consideration for FAIR) and a conversion of 10% of laser energy into the hot electron fraction. This order of magnitude is typically inferred from absolute measurements of the K-alpha emission (e.g., Myatt *et al*., 2007), whereas recent three-dimensional particle-in-cell simulations at intensities beyond 10^{20} W/cm^2 suggest even values exceeding 50% (Kemp *et al*., 2012).

To generate synthetic radiographic images, the Abel transform of the radial mass densities reported in Tahir *et al*. (2005) is performed and tabulated cold opacities are used to calculate the transmission. Use of cold opacities is justified as the attenuation at photon energies beyond the K-edge is dominated by photo-ionization of the K-shell, which is unaffected by the few-eV temperatures reached in the heavy-ion heated target, and Compton scattering, which is only dependent on the total electron density, and thus temperature independent. The simulated images include the shot noise due to the finite number of photons emitted per resolution element, the photon absorption statistics inside the target, and the quantum efficiency of the assumed detector.

Figure 2 shows simulated radiographic images of the lead target at various conditions: (Fig. 2a) heated liquid state, the target has been heated to a temperature of 3400–6000 K, while still at solid density; (Fig. 2b) the target has undergone expansion to conditions around the critical point ($T \approx 4000$ K, $\rho \approx 2$ g/cm^3); and (Fig. 2c) a smaller initial target, and further expansion to the strongly coupled plasma regime ($T \approx 5600$ K, $\rho \approx 4$ g/cm^3). Figure 2d shows the signal behind a calibration wedge, consisting of steps with thicknesses ranging from 20 to 600 μm, manufactured from the same material as the target. This method provides an absolute calibration allowing to directly relate the image exposure to the areal mass

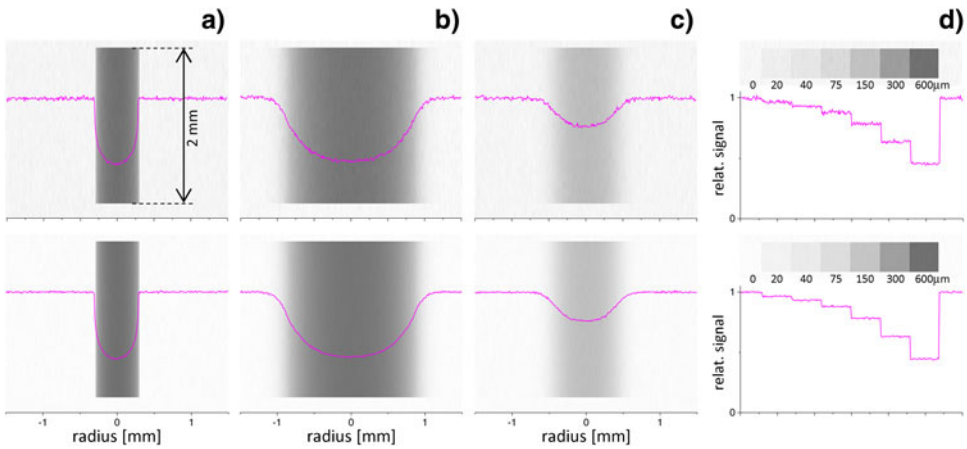

Fig. 2. Attenuation (dot-dashed) and fraction of deposited energy (solid line) within the sensitive layer, for SR-type imaging plate (red) and DRZ screen (blue), determined from Monte-Carlo calculations with GEANT4. Again, the transmission through 1 mm lead is shown (black).

https://doi.org/10.1017/S0263034614000652 Published online by Cambridge University Press

Table 1. *Detector parameters as used in the Monte-Carlo simulations for quantum efficiency and response*

Detector		Image Plate			DRZ screen		
Type		BAS-SR			DRZ-STD		
Vendor		Fujifilm			Mitsubishi Chemical Corporation		
	thickness	density	composition		thickness	density	composition
Supporting layer	≈200 μm	1.4 g/cm^3	Mylar		250 μm	1.4 g/cm^3	Mylar
Phosphor layer	112 μm	34 mg/cm^2	$BaFBrC_{2.364}H_{3.547}\ N_{0.591}O_{0.296}$		140 μm	68 mg/cm^2	Gd_2O_2S:Tb
Protection layer	8 μm	1.4 g/cm^3	Mylar		6 μm	1.4 g/cm^3	Mylar

density, and has been successfully employed by Brambrink *et al*. (2009). As can be seen, an average transmission of ≈ 50% at the maximum areal density in the target center provides a good image contrast. The signal-to-noise ratio (SNR) of around 60 suggests that absolute measurement of the areal density to a few percent levels can be achieved.

The detector assumed for calculating the radiographs in Figure 2 (top) was an imaging plate detector (SR-type, Fujifilm). Imaging plate detectors are widely used in medical imaging applications involving X- rays with energies up to 100 keV. The imaging plate is doped with a photostimulable phosphor which is excited to a metastable state upon deposition of energy by ionizing radiation, e.g., by X-ray photons. The stored information can later be retrieved by scanning the image plate with a laser scanner which de-excites the phosphor, resulting in emission of fluorescence light.

For a realistic assessment of the achievable SNR in the radiographic images, the detector quantum efficiency and response function over the relevant photon energy range (i.e., up to MeV) is needed. A good estimate for the detector quantum efficiency (i.e., the probability of a photon to make an interaction within the sensitive layer) and the detector response (i.e., the average amount of signal generated by a photon) can be obtained from the attenuation and the average amount of deposited energy per photon, respectively. We calculated these by means of Monte-Carlo simulations using the code suite GEANT4 (Agostinelli *et al*., 2003), detector parameters used in the calculations are listed in Table 1. Figure 3 (red, dot-dashed) shows the results obtained for the image plate. After an initial rise (due to the increasing transmission through the top protective layer) we find the interaction probability close to unity for photon energies up to about 20 keV. For higher photon energies, the interaction probability rapidly drops to about 5% and further to <1% for 100 keV and 200 keV, respectively. The jumps around 13.5 keV and 37 keV are due to the absorption K-edges of Bromine and Barium, respectively.

Also shown (solid line) is the fraction of energy a photon deposits on average within the sensitive layer. For small energies, this follows closely the interaction probability, as attenuation is dominated by photo-ionization and the resulting photo-electron will be stopped within the sensitive layer. For higher energies (beyond the K-shell absorption edges), the deposited energy fraction falls below the attenuation probability as an increasing amount of the initial photon energy can escape the sensitive layer (e.g., K-shell fluorescence photons, energetic photo electrons). In addition, in Compton scattering only a fraction of the photon energy is transferred in the interaction process.

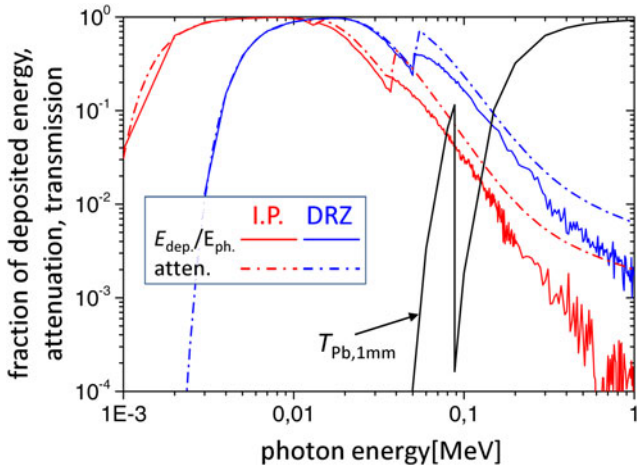

Fig. 3. Synthetic radiographs from various stages of a heavy-ion heated target (**a**–**c**), see text), and calibration wedge (**d**). The X-ray spectrum from Figure 1b was used with a total energy of 40 J in the hot electron distribution. Upper images assume an image plate detector, lower images using the DRZ-screen show improved signal-to-noise due to the increased quantum efficiency.

HARD X-RAY IMAGING DETECTOR DEVELOPMENT AND TESTS

Again, for reference, in Figure 3, the transmission through 1 mm of lead is plotted, showing that photons with energies beyond 100 keV are required for imaging such thick high-Z targets. The significant drop in quantum efficiencies for imaging plate detectors directly translates into to the need for the powerful X- ray source to achieve high-quality images with sufficient SNR. Increasing the detector quantum efficiency in this energy range would improve the photon statistics and thus allow more accurate density measurements, or alternatively, for a less energetic laser system to drive the X-ray source. As the quantum efficiency is directly related to the interaction probability within the sensitive layer, increasing thickness, density, and average atomic number are required.

https://doi.org/10.1017/S0263034614000652 Published online by Cambridge University Press

For comparison, we have calculated response and efficiency of a commercial fluorescent screen (DRZ-Std, Mitsubishi Chemical Corporation, parameters see Table 1) see Figure 3 (blue). We note that in these calculations the X-rays were assumed to enter the screen from the side of the supporting base, to view the fluorescence light through the thin protection layer. This leads to reduced efficiencies below 10 keV, which is uncritical for our envisioned application. In the relevant range above 100 keV, the quantum efficiency is approximately four times larger. Employing this increased efficiency the simulated radiographs (Fig. 2, bottom) show a SNR of approximately 120, an increase of two times as expected.

Conversion of X-ray radiation to visible light by scintillating screens, in combination with subsequent digitization by charge-coupled device arrays, also addresses another important requirement for detection systems at FAIR. Irradiation of massive targets with intense pulses of relativistic heavy-ions will lead to a considerable amount of activation of the experimental area close to the interaction. Access to the target area will therefore only be granted after a certain decay time (of the order of days) until this activation has "cooled down" to a level that again permits human activities. This is in contrast with the high repetition rates typical for accelerators, and also the laser system planned for FAIR will be designed to deliver several shots per hour. For this reason, detection schemes that require physical removal of the detector to access the experimental data (e.g., film, image plate) are strongly discouraged. Rather, detection systems should allow remote operation and electronic readout.

We have designed a first prototype of such a hard X-ray imaging detector (Fig. 4). Fluorescence from a DRZ screen is imaged by a combination of achromatic lenses (AC508-150-A, AC508-750-A, Thorlabs) onto a 12-bit charge-coupled device camera (Pixelfly QE, PCO). The lens system had been designed to provide a good balance between conflicting requirements for field-of-view, resolution, and light collection efficiency. The DRZ screen, optics, and optical path up to the camera are housed within black-anodized aluminum tubes to suppress background due to visible straylight. X-rays enter the housing through a 5 mm thick aluminum entrance "window," which acts as a high-pass, suppressing photons < 20 keV. A flat mirror in the optical path brings the charge-coupled device camera out of the direct view to the X-ray source so the sensitive electronics can be heavily shielded.

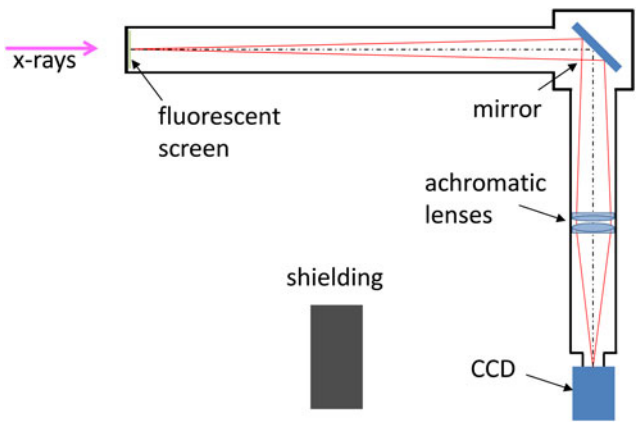

Fig. 4. Schematic of the prototype hard X-ray imager (details see text).

First tests were performed at the superconducting electron linear accelerator S-DALINAC (University of Darmstadt, Darmstadt, Germany). Electron beams at 6.5 MeV energy produced bremsstrahlung in a thick copper converter target. Using currents of 9.25 μA and an exposure time of 10 s, high quality radiographic images were obtained (Figs. 5a and 5b), even penetrating tantalum blocks up to 24 mm in thickness. At the high-energy laser facility PHELIX (Bagnoud *et al*., 2010) at GSI, we employed hard X-ray sources as discussed in the previous sections, i.e., driven by the energetic high-intensity laser pulses. Pulses with energies up to 100 J in 500 fs were focused onto thin metal foils and radiographs of various objects (M4 steel nut, Ta-slabs) were obtained.

In these measurements, the test objects were located close to the scintillator so that the detector's overall spatial resolution could be assessed. We find a resolution of the order of 150 μm. Detailed optical ray-tracing analysis indicates that the resolution is mainly limited by the remaining spherical aberrations. Nevertheless, the useful field-of-view of 40 mm provides more than 250 resolution elements. To achieve a resolution at the target of 10 μm (the lower limit due to the source size) would require a magnification of 15, i.e., a distance of 15 cm between target and detector. The field-of-view of about 2.5 mm matches well the typical target dimensions (cf. Fig. 2).

Our Monte Carlo simulations suggest that lateral spreading of the deposited energy in the scintillating layer is less than or equal to 10 μm, i.e., small compared to the resolution of our optical system. We therefore expect that the overall spatial resolution could be significantly improved by use of coherent fiber bundles with individual fiber diameters of 10 μm to transport the scintillation light from the screen to the charge-coupled device. At the same time, close coupling would increase the light collection efficiency by a factor 100 which would greatly improve the SNR achieved by the charge-coupled device camera.

While the use of a DRZ screen already leads to an increase in quantum efficiency by four times compared to imaging plates, even further increase should be achievable when using thick (≈ 500 μm) heavy scintillation crystals, e.g., BGO (Bismuth germinate) or LYSO (Cerium-doped Lutetium Yttrium Orthosilicate). These options will be explored in future work.

CONCLUSIONS

Through simulated radiographs of heavy-ion heated targets proposed within the FAIR plasma physics experimental program, we have shown that high-energy laser driven hard

https://doi.org/10.1017/S0263034614000652 Published online by Cambridge University Press

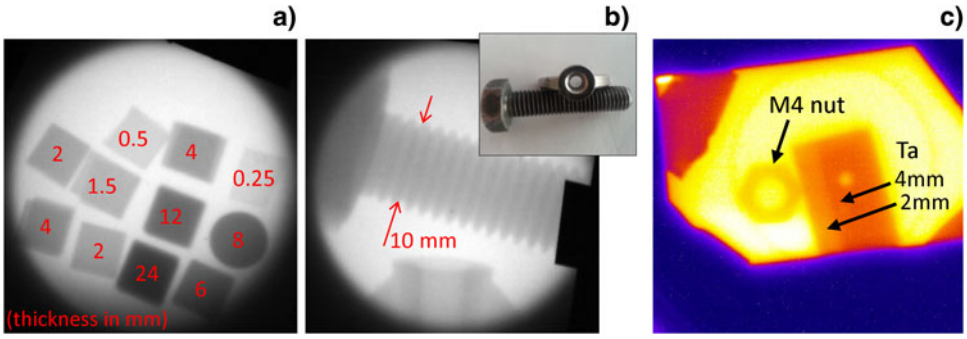

Fig. 5. Radiographs obtained with the hard X-ray imager at the S-DALINAC electron accelerator (a, b) and at the PHELIX laser facility (c). The test objects are tantalum blocks of various thicknesses (**a**), M10 steel screw (**b**), and M4 steel nut and tantalum slabs (**c**).

X-ray sources fulfil the requirements to produce high-quality radiographic images. This provides a strong case for a high-energy high-intensity laser installation at FAIR to enable this indispensable diagnostic capability. At the same time this will allow a variety of other X-ray diagnostic techniques, being routinely employed in state-of-the-art HED facilities, such as X-ray diffraction, absorption spectroscopy or Thomson scattering (Riley *et al*., 2007).

Development of high repetition rate X-ray imaging detectors with increased quantum efficiencies at photon energies beyond 100 keV show promising first results. Development towards thicker scintillators and fiber-based image transport is expected to further improve their performance.

ACKNOWLEDGEMENTS

We gratefully acknowledge support by the PHELIX laser and operations team. We thank Prof. Dr. N. Pietralla (TU Darmstadt) for the opportunity to perform tests at the S-DALINAC. This work was supported by the Alliance Program of the Helmholtz Association (HA216/EMMI).

REFERENCES

Agostinelli, S., Allison, J., Amako, K., Apostolakis, J., Araujo, H., Arce, P., Asai, M., Axen, D., Banerjee, S., Barrand, G., et al.. (2003). Geant4—A simulation toolkit. *Nucl. Instr. Meth. A* **506**, 250–303.

Bagnoud, V., Aurand, B., Blazevic, A., Borneis, S., Bruske, C., Ecker, B., Eisenbarth, U., Fils, J., Frank, A., Gaul, E., Goette, S., Haefner, C., Hahn, T., Harres, K., Heuck, H.-M., Hochhaus, D., Hoffmann, D.H.H., Javorkova, D., Kluge, H.-J., Kuehl, T., Kunzer, S., Kreutz, M., Merz-Mantwill, T., Neumayer, P., Onkels, E., Reemts, D., Rosmej, O., Roth, M., Stoehlker, T., Tauschwitz, A., Zielbauer, B., Zimmer, D. & Witte, K. (2010). Commissioning and early experiments of the PHELIX facility. *Appl. Phys. B* **100**, 137–150.

Beg, F.N., Bell, A.R., Dangor, A.E., Danson, C.N., Fews, A.P., Glinsky, M.E., Hammel, B.A., Lee, P., Norreys, P.A. & Tatarakis, M. (1997). A study of picosecond laser–solid interactions up to 10^{19} W cm^{-2}. *Phys. Plasmas* **4**, 447–457.

Brambrink, E., Wei, H.G., Barbrel, B., Audebert, P., Benuzzi-Mounaix, A., Boehly, T., Endo, T., Gregory, C.D., Kimura, T., Kodama, R., Ozaki, N., Park, H.-S. & Koenig, M. (2009). Direct density measurement of shock-compressed iron using hard x rays generated by a short laser pulse. *Phys. Rev. E* **80**, 056407/1–5.

Henning, W.F. (2004). The future GSI facility. *NIM B* **214**, 211–215.

Hicks, D.G., Spears, B.K., Braun, D.G., Olson, R.E., Sorce, C.M., Celliers, P.M., Collins, G.W. & Landen, O.L. (2010). Convergent ablator performance measurements. *Phys. Plasmas* **17**, 102703/1–11.

Hochhaus, D.C., Aurand, B., Basko, M., Ecker, B., Kühl, T., Ma, T., Rosmej, F., Zielbauer, B. & Neumayer, P. (2013). X-ray radiographic expansion measurements of isochorically heated thin wire targets. *Phys. Plasmas* **20**, 062703/1–7.

Hoffmann, D.H.H., Blazevic, A., Ni, P., Rosmej, O., Roth, M., Tahir, N.A., Tauschwitz, A., Udrea, S., Varentsov, D., Weyrich, K. & Maron, Y. (2005). Present and future perspectives for high energy density physics with intense heavy ion and laser beams. *Laser Part. Beams* **23**, 47–53.

Kemp, A.J. & Divol, L. (2012). Interaction physics of multipicosecond petawatt laser pulses with overdense plasma. *Phys. Rev. Lett.* **109**, 195005/1–5.

Kritcher, A.L., Döppner, T., Swift, D., Hawreliak, J., Collins, G., Nilsen, J., Bachmann, B., Dewald, E., Strozzi, D., Felker, S., Landen, O.L., Jones, O., Thomas, C., Hammer, J., Keane, C., Lee, H.J., Glenzer, S.H., Rothman, S., Chapman, D., Kraus, D., Neumayer, P. & Falcone, R.W. (2014). Probing matter at Gbar pressures at the NIF. *High Energy Density Physics* **10**, 27–34.

Le Pape, S., Neumayer, P., Fortmann, C., Döppner, T., Davis, P., Kritcher, A., Landen, O. & Glenzer, S.H. (2010). X-ray radiography and scattering diagnosis of dense shock-compressed matter. *Phys. Plasmas* **17**, 056309/1–9.

Lomonosov, I.V. (2007). Multi-phase equation of state for aluminium. *Laser Part. Beams* **25**, 567–584.

Myatt, J.,Theobald, W., Delettrez, J.A., Stoeckl, C., Storm, M., Sangster, T.C., Maximov, A.V. & Short, R.W. (2007). High-intensity laser interactions with mass-limited solid targets and implications for fast- ignition experiments on OMEGA EP. *Phys. Plasmas* **14**, 056301/1–8.

Neumayer, P., Aurand, B., Basko, M., Ecker, B., Gibbon, P., Hochhaus, D.C., Karmakar, A., Kazakov, E., Kühl, T., Labaune, C., Rosmej, O., Tauschwitz, An., Zielbauer, B. & Zimmer, D. (2010). The role of hot electron refluxing in laser-generated K-alpha sources. Phys. *Plasmas* **17**, 103103/1–7.

https://doi.org/10.1017/S0263034614000652 Published online by Cambridge University Press

Nilson, P.M., Davies, J.R., Theobald, W., Jaanimagi, P.A., Mileham, C., Jungquist, R.K., Stoeckl, C., Begishev, I.A., Solodov, A.A., Myatt, J.F., Zuegel, J.D., Sangster, T.C., Betti, R. & Meyerhofer, D.D. (2012). Time-resolved measurements of hot-electron equilibration dynamics in high-intensity laser interactions with thin-foil solid targets. *Phys. Rev. Lett.* **108**, 085002/1–5.

Park, H.-S., Chambers, D.M., Chung, H.-K., Clarke, R.J., Eagleton, R., Giraldez, E., Goldsack, T., Heathcote, R., Izumi, N., Key, M.H., King, J.A., Koch, J.A., Landen, O.L., Nikroo, A., Patel, P.K., Price, D.F., Remington, B.A., Robey, H.F., Snavely, R.A., Steinman, D.A., Stephens, R.B., Stoeckl, C., Storm, M., Tabak, M., Theobald, W., Town, R.P.J., Wickersham, J.E. & Zhang, B.B. (2006). High-energy K-alpha radiography using high-intensity, short-pulse lasers. *Phys. Plasmas* **13**, 056309/1–10.

Park, H.-S., Maddox, B.R., Giraldez, E., Hatchett, S.P., Hudson, L.T., Izumi, N., Key, M.H., Le Pape, S., MacKinnon, A.J., MacPhee, A.G., Patel, P.K., Phillips, T.W., Remington, B.A., Seely, J.F., Tommasini, R., Town, R., Workman, J. & Brambrink, E. (2008). High-resolution 17–75 keV backlighters for high energy density experiments. *Phys. Plasmas* **15**, 072705/1–9.

Riley, D., Khattak, F.Y., Garcia Saiz, E., Gregori, G., Bandyopadhyay, S., Notley, M., Neely, D., Chambers, D., Moore, A. & Comley, A. (2007). Spectrally resolved X-ray scatter from laser-shock-driven plasmas. *Laser Part. Beams* **25**, 465–469.

Spiller, P. & Franchetti, G. (2006). The FAIR accelerator project at GSI. *NIM A* **561**, 305–309.

Tahir, N.A., Deutsch, C., Fortov, V.E., Gryaznov, V., Hoffmann, D.H.H., Kulish, M., Lomonosov, I.V., Mintsev, V., Ni, P., Nikolaev, D., Piriz, A.R., Shilkin, N., Spiller, P., Shutov, A., Temporal, M., Ternovoi, V., Udrea, S. & Varentsov, D. (2005). Proposal for the study of thermophysical properties of high-energy-density matter using current and future heavy-ion accelerator facilities at GSI Darmstadt. *Phys. Rev. Lett.* **95**, 035001/1–4.

Tahir, N.A., Stöhlker, Th., Shutov, A., Lomonosov, I.V., Fortov, V.E., French, M., Nettelmann, N., Redmer, R., Piriz, A.R., Deutsch, C., Zhao, Y., Zhang, P., Xu, H., Xiao, G. & Zhan, W. (2010). Ultrahigh compression of water using intense heavy ion beams: laboratory planetary physics. *New J. Phys.* **12**, 073022/1–17.

Tauschwitz, An., Novikov, V.G., Tauschwitz, A. Rosmej, F.B., Abdallah, J., Onkels, E., Jacoby, J. & Maruhn, J.A. (2009). Intense ion beams as a tool for opacity measurements in warm dense matter. *Appl. Phys. B* **95**, 13–16.

Tommasini, R., Hatchett, S.P., Hey, D.S., Iglesias, C., Izumi, N., Koch, J.A., Landen, O.L., MacKinnon, A.J., Sorce, C., Delettrez, J.A., Glebov, V.Yu., Sangster, T.C. & Stoeckl, C. (2011). Development of Compton radiography of inertial confinement fusion implosions. *Phys. Plasmas* **18**, 056309/1–7.

Zastrau, U., Audebert, P., Bernshtam, V., Brambrink, E., Kämpfer, T., Kroupp, E., Loetzsch, R., Maron, Y., Ralchenko, Yu., Reinholz, H., Röpke, G., Sengebusch, A., Stambulchik, E., Uschmann, I., Weingarten, L. & Förster, E. (2010). Temperature and Kα-yield radial distributions in laser-produced solid-density plasmas imaged with ultrahigh-resolution X-ray spectroscopy. *Phys. Rev. E* **81**, 026406/1–4.

Zastrau, U., Burian, T., Chalupsky, J., Döppner, T., Dzelzainis, T.W.J., Fäustlin, R.R., Fortmann, C., Galtier, E., Glenzer, S.H., Gregori, G., Juha, L., Lee, H.J., Lee, R.W., Lewis, C.L.S., Medvedev, N., Nagler, B., Nelson, A.J., Riley, D., Rosmej, F.B., Toleikis, S., Tschentscher, T., Uschmann, I., Vinko, S.M., Wark, J.S., Whitcher, T. & Förster, E. (2012). XUV spectroscopic characterization of warm dense aluminum plasmas generated by the free-electron-laser FLASH. *Laser Part. Beams* **30**, 45–56.

https://doi.org/10.1017/S0263034614000652 Published online by Cambridge University Press